Taylor & Francis
Taylor & Francis Group

Aerosol Science and Technology

ISSN: (Print) (Online) Journal homepage: https://www.tandfonline.com/loi/uast20

Estimating mass-absorption cross-section of ambient black carbon aerosols: Theoretical, empirical, and machine learning models

Hanyang Li & Andrew A. May

To cite this article: Hanyang Li & Andrew A. May (2022) Estimating mass-absorption cross-section of ambient black carbon aerosols: Theoretical, empirical, and machine learning models, Aerosol Science and Technology, 56:11, 980-997, DOI: 10.1080/02786826.2022.2114311

To link to this article: https://doi.org/10.1080/02786826.2022.2114311

AEROSOL SCIENCE AND TECHNOLOGY
2022, VOL. 56, NO. 11, 980–997
https://doi.org/10.1080/02786826.2022.2114311

OPEN ACCESS Check for updates

Estimating mass-absorption cross-section of ambient black carbon aerosols: Theoretical, empirical, and machine learning models

Hanyang Li[a,b] and Andrew A. May[a]

[a]Department of Civil, Environmental, and Geodetic Engineering, The Ohio State University, Columbus, Ohio, USA; [b]Department of Civil, Construction, and Environmental Engineering, San Diego State University, San Diego, California, USA

ABSTRACT
The mass-absorption cross-section of black carbon (MAC_{BC}) is an essential parameter to link the atmospheric concentration of black carbon (BC) with its radiative forcing. When a direct calculation of MAC_{BC} based on observations of aerosol light absorption and BC mass concentration is impossible, we rely on modeling and simulations to estimate MAC_{BC}, but currently, there is no consensus model that can be relied on for accurate predictions across all atmospheric environments when BC particles have different coating thicknesses. Here, we applied five MAC_{BC} prediction models (including three light scattering theories, an empirical model based on observations of particle mass concentrations, and a machine learning model developed in our previous work) to aerosols from three Department of Energy (DOE) Atmospheric Radiation Measurement (ARM) field campaigns. While many studies have found that increasing the complexity of the models helps to constrain biases of the estimated MAC_{BC}, our effort is to evaluate the models based on the criteria of simplicity and accuracy. We find that our machine learning model (support vector machine for regression, SVM) generally performs well across all DOE ARM field campaign data, while the accuracy of core-shell Mie theory depends on the bias correction algorithm applied to filter-based light absorption data. Generally, the empirical model for internally mixed particles that we considered tends to over-predict MAC_{BC}, while Mie theory for externally mixed particles tends to under-predict MAC_{BC}. An examination of the influence of coating material on BC cores suggests that the performance of our current SVM model is degraded when the BC is thickly coated (e.g., it has undergone aging and mixing with other materials in the atmosphere).

ARTICLE HISTORY
Received 3 March 2022
Accepted 15 July 2022

EDITOR
Hans Moosmüller

Introduction

Black carbon (BC) has an important and complex, yet uncertain, role in the climate system (Bond et al. 2013). Multiple approaches exist to quantify atmospheric BC, but these are operationally defined (Lack et al. 2014; Petzold et al. 2013). Herein, we focus on aerosol light absorption measurements, which typically either quantify light attenuation through a filter or utilize a photoacoustic technique. These instruments provide an aerosol light absorption coefficient (B_{abs}) at the wavelength(s) of light at which the measurement occurs. Measurements of B_{abs} (and absorption aerosol optical depth) are often used to evaluate predictions of aerosol radiative forcing in chemistry-climate models (e.g., Gliß et al. 2021). However, the challenge is that BC emissions within these models are mass-based (e.g., Tg year^{-1}, as in Bond et al. [2013] and McDuffie et al. [2020]), so a conversion between B_{abs} and BC mass concentration (M_{BC}) is required for model evaluation. Often, this conversion factor is referred to as the mass-absorption cross-section of BC (MAC_{BC}), that is, $B_{abs} = MAC_{BC} \cdot M_{BC}$.

There are several approaches that one can follow to define a value of MAC_{BC}. With observations of both B_{abs} and M_{BC}, one can derive observed values of MAC_{BC} at a given wavelength of light (λ) through time and/or space (Yuan et al. 2021; Cho et al. 2019; Cross et al. 2010). In the absence of experimental observations, MAC_{BC} has traditionally been assumed to be $7.5 \pm 1.2\,m^2\,g^{-1}$ at 550 nm based on the classical review of mostly laboratory studies by Bond and Bergstrom (2006); in a separate review of studies occurring after 2006, Liu et al. (2020) obtained a similar value ($8.0 \pm 0.7\,m^2\,g^{-1}$ at 550 nm). To extend MAC_{BC} to

CONTACT Andrew A. May may.561@osu.edu Department of Civil, Environmental, and Geodetic Engineering, The Ohio State University, Columbus, Ohio, USA
Supplemental data for this article can be accessed online at https://doi.org/10.1080/02786826.2022.2114311

different wavelengths, a power-law function is often used:

$$MAC_{BC}(\lambda) = MAC_{BC}(550\ nm) \cdot \left(\frac{\lambda}{550\ nm}\right)^{-AAE_{BC}} \quad (1)$$

where AAE_{BC} is the absorption Ångström exponent for BC. The value of AAE_{BC} is frequently assumed to be 1 (Lack and Langridge 2013; Bergstrom, Russell, and Hignett 2002), although this value varies in the literature depending on the adopted method. For example, Bahadur et al. (2012) obtained a value of 0.6 from satellite data, while Gyawali et al. (2017) used core-shell Mie theory to infer a value of 1.7. However, many analyses of field data that provide more direct estimates of AAE_{BC} suggest that this value falls between roughly 0.9 and 1.5 (e.g., Li and May 2020a; Saturno et al. 2017; Cappa et al. 2016; Backman et al. 2014).

In this work, we focus on 870 nm, specifically, because it is the operating wavelength of one model of the Droplet Measurement Technologies Photoacoustic Extinctiometer, which we have used in prior work (Li, McMeeking, and May 2020). Thus, if we propagate these uncertainties in both MAC_{BC} and AAE_{BC} through Equation (1) to predict MAC_{BC} at 870 nm by assuming that MAC_{BC} at 550 nm is represented by a normal distribution ($7.5 \pm 1.2\ m^2\ g^{-1}$) and AAE_{BC} is represented by a linear distribution bounded by 0.6 and 1.7, we obtain a value of $4.46 \pm 0.98\ m^2\ g^{-1}$; the assumption of a normal distribution for AAE_{BC} (1.1 ± 0.3) yields similar values of $4.56 \pm 0.94\ m^2\ g^{-1}$. Moreover, BC likely dominates light absorption at 870 nm. Tar-like brown carbon has a MAC of roughly $1\ m^2\ g^{-1}$ (Corbin et al. 2019), while mineral dust has a MAC of roughly $0.05\ m^2\ g^{-1}$ (Caponi et al. 2017), so large quantities of these other absorbing aerosols (relative to BC) are required to influence MAC_{BC}.

However, experimentally derived values of MAC_{BC} from field observations do not always agree with these "community standards" of MAC_{BC} and AAE_{BC}. Specifically, for ambient aerosols, MAC_{BC} has been reported within the range of $2.3–15\ m^2\ g^{-1}$ at 550 nm (Mbengue et al. 2021; Ohata et al. 2021; Yuan et al. 2021; Cho et al. 2019; Gyawali et al. 2017; Zanatta et al. 2016; Nordmann et al. 2013; Kondo et al. 2011; Moosmüller et al. 1998), and we previously reported values between roughly 3 and $4\ m^2\ g^{-1}$ at 870 nm (Li and May 2020a). There is similar variable agreement among laboratory studies of torch-generated BC particles (e.g., Cross et al. 2010; Scarnato et al. 2013; Forestieri et al. 2018).

Variations in MAC_{BC} may exist for a myriad of reasons. If the BC is internally mixed with other aerosol components, its light absorption may be enhanced (Yuan et al. 2021; Conrad and Johnson 2019; Lack and Cappa 2010; Bond, Habib, and Bergstrom 2006; Jacobson 2001), but these mixtures are non-homogeneous (Fierce et al. 2016, 2020; Zhang et al. 2017; Moteki, Kondo, and Adachi 2014; Adachi, Chung, and Buseck 2010). Values of absorption enhancement (E_{abs}) can be determined by measuring MAC before and after removal of particles' coating in a thermodenuder (Lack et al. 2014; Cappa et al. 2012; Knox et al. 2009), and previous studies observed a broad range E_{abs} (1.06–4.5) due to different experimental conditions (Wei et al. 2020). Similarly, the morphology (e.g., density, shape, and size distribution) of the BC particles influences their light absorption (Wu et al. 2018; Zhang et al. 2008). During atmospheric transport of BC, chemical aging may alter MAC_{BC} (Xu et al. 2018; Subramanian et al. 2010; Zaveri et al. 2010; Knox et al. 2009), likely due to transformations to the BC mixing state and/or its morphology. Electronic microscopy can provide the accurate measurement of BC aggregates and their mixing with other materials (Wang et al. 2021), but it remains difficult to capture the change of BC morphology across the whole aging process. Consequently, some studies have proposed the use of location-specific MAC_{BC} (Srivastava et al. 2021; Ram and Sarin 2009).

When constrained by observations, a number of theoretical approaches have the potential to etimate MAC_{BC} at a given incident wavelength of light. Core-shell Mie theory serves as one approach for estimating optical properties of internally mixed BC through the assumption of spherical BC cores that are uniformly coated by organic and inorganic components (Jacobson 2000; Bohren and Huffman 1983). Likewise, Mie theory can be applied to external mixtures of BC and other components (Li et al. 2019; Lesins, Chylek, and Lohmann 2002). Another commonly used theoretical approach is the Rayleigh-Debye-Gans approximation for fractal aggregates (RDG-FA) (Conrad and Johnson 2019; Sorensen 2001; Dobbins and Megaridis 1991). In the RDG-FA approach, the total absorption of an aggregate is the sum of absorption of individual BC spherules. For any theoretical approach, its accuracy is sensitive to the required input parameters, such as BC refractive index, particle morphology, and particle mixing state, all of which are difficult and/or labor-intensive to measure (Liu et al. 2020; Forestieri et al. 2018; Zanatta et al. 2018; García Fernández, Picaud, and Devel 2015; Lack and Cappa 2010). However, even if these parameters can be measured accurately, the theoretical formulations may not truly capture all of the underlying physics (Bond and Bergstrom 2006).

To address potential challenges related to an incomplete understanding of the underlying physics, several prior studies have developed empirical models describing the relationship between MAC_{BC} and other observed aerosol-related parameters. For example, based on the observational relationship between the MAC_{BC} of flare-generated BC and key flare parameters (e.g., flare temperature, volumetric flow rate, and carbon-hydrogen ratio), Conrad and Johnson (2019) modeled MAC_{BC} at 550 nm as a power-law equation (cf., their Equation 5). Similarly, Chakrabarty and Heinson (2018) examined the relationship between MAC_{BC} and the ratio of total particle mass to BC mass for both observational and simulated data of BC particles, and they proposed an empirical model (cf., discussion of their Figure 2; our Equation (6) below). Likewise, to improve the parametrization of BC absorption in climate models, Wu et al. (2018) suggested a correction of E_{abs} using an exponential function (cf., their Figure S13). Overall, these empirical models provide straightforward and computationally inexpensive methods toward improving the prediction accuracy of BC radiative forcing. However, building these models requires the assumption of a functional relationship between the independent and dependent variables, which is often subjective unless there is an underlying physical model. Furthermore, since the empirical models are typically simple in their structure, their accuracy may degrade when the experimental conditions are different from the one where the model is generated.

To mitigate uncertainties in MAC_{BC} related to assumptions related to the appropriate theoretical formulation and aerosol properties, we previously applied different data-driven approaches to predict MAC_{BC} at 870 nm for ambient and biomass burning aerosols (Li and May 2020a). We differentiate this approach from the aforementioned empirical models because our data mining method seeks to discover unexpected patterns and identify hidden relationships in the datasets with no pre-defined mathematical model. As described in Li and May (2020a), our models use temporally varying aerosol properties, namely observations of B_{abs}, aerosol light scattering coefficients (B_{scat}), and number and volume size distributions, as input variables to the models in the prediction of time series of MAC_{BC}. The models were constructed using ambient aerosols from the US Department of Energy (DOE) Atmospheric Radiation Measurement (ARM) Two-Column Aerosol Project (TCAP) and then applied to two independent validation datasets: the DOE ARM Cloud, Aerosol, and Complex Terrain Interactions (CACTI) project and the 2016 FireLab component of the Fire Influence on Regional to Global Environments and Air Quality (FIREX-AQ) campaign, which was sponsored by the US National Oceanic and Atmospheric Administration. Based on the model performance metrics in Li and May (2020a) and an extended uncertainty evaluation in May and Li (2022), we put forth support vector machine (SVM) for regression as the recommended technique for use.

In this work, we present an expanded evaluation of our SVM model on the prediction of MAC_{BC} for ambient aerosols from different atmospheric environments around the world, including CACTI, the DOE ARM Observations and Modeling of the Green Ocean Amazon (GOAMAZON) project, and the DOE ARM Layered Atlantic Smoke Interactions with Clouds (LASIC) project. Furthermore, we systematically compare the MAC_{BC} estimated by our model and existing theoretical and empirical approaches, including some that account for the enhancement to aerosol light absorption that may occur when BC is internally mixed, in order to compare our machine-learning model to established approaches and to assess the generalizability of our model.

Methodology

Within this section, we describe three different approaches to predict MAC_{BC}, namely SVM, theoretical, and empirical models, along with a description of the observational data that were used for model evaluation.

SVM modeling

We provide a detailed discussion of our machine learning model in Li and May (2020a). Briefly, SVM maps independent variables into a higher-dimensional space where linear regression is performed (Smola and Schölkopf 1998; Drucker et al. 1997; Cortes and Vapnik 1995). Fundamentally, the SVM approach selects a subset of observations from the training dataset as "support vectors" to define the margins of hyperplanes for the model (and to discard "unwanted" data samples), which makes the model robust to data noise and applicable to datasets with substitution of input variables. SVM can handle non-linear problems through the use of non-linear kernels, and it is less prone to over-fitting than other regression techniques. Our selection of the hyperplane and kernel function

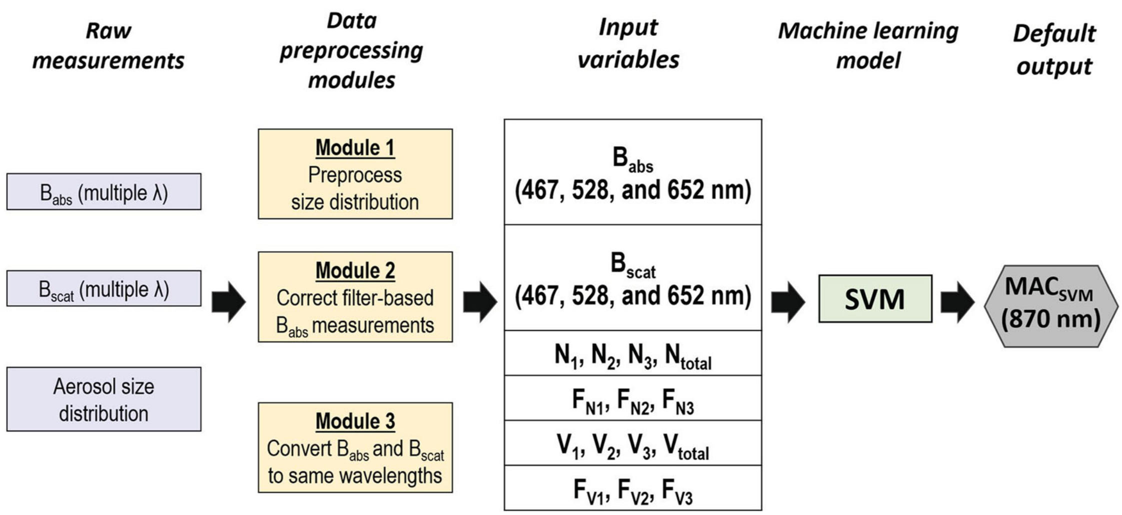

Figure 1. Schematic flow chart showing the flow for estimating MAC_{SVM} at 870 nm. N_1, N_2, and N_3 represent the aerosol number concentration falling within the size class bins (<50 nm, 50–200 nm, and >200 nm), while V_1, V_2, and V_3 represent the aerosol volume concentration within the size class bins (<1000 nm, 1000–2500 nm, and >2500 nm). The sum of the N_i and V_i values equals the total aerosol number or volume concentrations (N_{total} and V_{total}). F_{j1}, F_{j2}, and F_{j3} represent the fraction of total aerosol concentration falling within each class for either number (F_{Ni}) or volume (F_{Vi}), and by definition, the sum of both F_{Ni} and F_{Vi} equals 1. See the online version for a colorized figure.

can be found in the supplementary materials of Li and May (2020a). However, SVM is not without limitation; for example, it is more computationally expensive than linear regression, and it may be difficult to interpret the derived regression model. In addition, SVM can have large prediction errors when extrapolating beyond the training parameter space; in other words, the extrapolation of SVM to unseen data remains uncertain.

We designed our SVM model with the intent to utilize aerosol measurements common to many observational sites in its prediction of MAC_{BC}; moreover, we selected the input variables to emulate light scattering theories. For example, because Mie theory requires particle size as an input, we incorporated particle number distributions and particle volume distributions as candidate variables for our models. Similarly, we considered observations of B_{abs} and B_{scat} as proxies for aerosol composition, because they are widely measured and their spectral dependencies (i.e., AAE and the scattering Ångström exponent or SAE) have been used to categorize absorbing aerosols by type (Cappa et al. 2016; Cazorla et al. 2013).

Prior to input to the SVM model, the aerosol measurements are pre-processed to apportion the particle number and volume size distributions into a few size bins; to apply correction factors to filter-based absorption photometer data using either Bond, Anderson, and Campbell (1999) or Li, McMeeking, and May (2020); and to convert B_{abs} and B_{scat} to "standard" wavelengths that are used in filter-based absorption photometers common to many long-term ground sites (467, 528, and 652 nm in our model). These pre-processing steps have been detailed described in Li and May (2020a) and are available in an online repository (Li and May 2020b). We ultimately input 20 candidate variables into the model to determine MAC_{BC} at 870 nm (referred to as MAC_{SVM} in Figure 1).

Theoretical modeling

We considered two commonly used theoretical models: the RDG-FA approximation and Mie theory. In general, the RDG-FA approximation for MAC_{BC} can be expressed as:

$$MAC_{RDG}(\lambda) = \frac{6\pi}{\rho} \cdot \frac{E(m(\lambda))}{\lambda} \tag{2}$$

where $E(m(\lambda) = Imag\left(\frac{m^2-1}{m^2+2}\right)$, ρ is the material density of BC (1.8 g cm^{-3}), m is the complex refractive index of BC, and λ is the wavelength of light (870 nm in the present work). When using m = 1.95 + 0.79i as recommended by Bond and Bergstrom (2006), MAC_{RDG} is 3.06 m^2 g^{-1} at 870 nm. However, as discussed in Liu et al. (2020), a correction factor (0.9 to 1.3) appears to be necessary to account for the variation in BC particle sizes and refractive indices; consequently, MAC_{RDG} ranges from 2.75 to 3.98 m^2 g^{-1} in our analyses. At 550 nm, we calculate MAC_{RDG} ranging from 4.4 to 6.3 m^2 g^{-1}. These results are 29 ± 13%

lower than the most widely cited MAC_{BC} value of $7.5\,m^2\ g^{-1}$ at 550 nm (Bond and Bergstrom 2006), suggesting an uncertainty in either the RDG-FA model itself or the properties of BC particle used in the approximation. Probing a range of m within any theoretical model is outside the scope of our analysis.

Within Mie theory, we examined two bounding cases for spherical BC particles: a purely external mixture and a core-shell internal mixture. For both mixing states, the general form to calculate MAC_{BC} is:

$$MAC_{Mie} = \frac{B_{abs}\ (Mie\ theory)}{mass_{BC}\ (SP2)} = \frac{\int_0^{\infty} \frac{\pi d_p^2}{4} n(d_p)\ Q_{abs}\ d(d_p)}{mass_{BC}\ (SP2)} \quad (3)$$

where $mass_{BC}$ is the BC mass concentration (here, taken from a Droplet Measurement Technologies Single Particle Soot Photometer, or SP2), Q_{abs} is the calculated dimensionless absorption efficiency of a single BC particle, d_p is the diameter of particle detected by the SP2 (15 to 550 nm, with a bin size of 5 nm), and $n(d_p)$ is the SP2-derived size distribution. We selected this lower bound because the raw data from the DOE ARM Data Discovery website include SP2 number distributions spanning this range in 5 nm bins.

The calculations of B_{abs} and Q_{abs} were performed using the PyMieScatt library in Python (Sumlin, Heinson, and Chakrabarty 2018). To calculate B_{abs} with an assumption of externally mixed particles, we applied the function of *Mie_SD* in the library. Specifically, the program first computes Q_{abs} for each single, homogeneous particle with a refractive index of 1.95 + 0.79i (the same value as in the RDG-FA model) at a wavelength of 870 nm, then integrates numerically over binned SP2 size distribution data to obtain B_{abs}.

For the case of internally mixed particles, we followed a two-step approach. In the first step, we used the function of *MieQCoreShell* from Sumlin, Heinson, and Chakrabarty (2018) to derive Q_{abs}, where we assumed a refractive index of 1.5 + 1e-4i (i.e., non-absorbing) for the coating materials (Saliba et al. 2016; Schnaiter et al. 2005) and a refractive index of 1.95 + 0.79i for the BC core. We used the same refractive indices as those chosen to obtain the empirical model as described in Chakrabarty and Heinson (2018), so we can compare the predicted MAC_{BC} between the methods. To determine the shell diameter, we followed Saliba et al. (2016), who assumed that the coating is solely attributed to the difference between Scanning Mobility Particle Sizer (SMPS) and SP2 particle size distributions and the shell diameter ($d_{p.shell}$ (i)) is a function of core diameter ($d_{p.SP2}$ (i)) and the volume ratio of the shell and the BC core:

$$d_{p.shell}\ (i) = d_{p.SP2}\ (i)\ \times \left(\frac{volume_{shell}}{volume_{BC}}\right)^{1/3} \quad (4)$$

With the measurements of SMPS and SP2, Equation (4) becomes

$$d_{p.shell}\ (i) = \left(\frac{\rho_{BC}}{\rho_{coating}}\ \frac{mass_{coating}}{mass_{BC}\ (SP2)} + 1\right)^{1/3} d_{p.SP2}\ (i) \quad (5)$$

where $mass_{coating}$ is defined as:

$$mass_{coating} = \rho_{coating}\ (volume_{SMPS} - volume_{SP2}) \quad (6)$$

with $volume_{SMPS} = \sum \frac{\pi}{6}\ d_{p.SMPS}^3\ n(d_p)$ and $volume_{SP2} = mass_{BC}\ (SP2)/\rho_{BC}$. The values of $\rho_{coating}$ and ρ_{BC} were assumed to be 1.2 and 1.8 g cm^{-3}, respectively, as in Saliba et al. (2016).

In the second step of the calculation, Q_{abs} was integrated using the *scipy.integrate.trapz* function in the Scipy library (Varoquaux et al. 2015) to obtain B_{abs} (the numerator of Equation (3)). Hereafter, we use the term $MAC_{Mie.ext}$ and $MAC_{Mie.int}$ to represent the MAC_{BC} derived for external and internal mixing states, respectively.

Empirical modeling

We only considered the empirical model that was developed by Chakrabarty and Heinson (2018), because the inputs to this model are available within our data. This model was developed for BC with different internally mixed morphologies (i.e., bare, partly coated, and embedded aggregates), and this diversity suggests applicability to both fresh and aged BC particles in the atmosphere. Following the power-law scaling relation defined by this model, we calculated empirical MAC_{BC} as expressed in Equation (7):

$$MAC_{empircal} = \frac{3.6}{\lambda} \left(\frac{mass_{total}(SMPS)}{mass_{BC}(SP2)}\right)^{1/3} \quad (7)$$

where λ is the wavelength in μm and $mass_{total}$ (SMPS) is the inferred mass concentration of particles from an SMPS. Therefore, for pure BC particles ($mass_{total}(SMPS)/mass_{BC}(SP2) = 1$), this model predicts $MAC_{BC} = 4.14\,m^2\ g^{-1}$ at 870 nm, and when $mass_{total}(SMPS)/mass_{BC}(SP2) > 1$, the model predicts that light absorption will be enhanced.

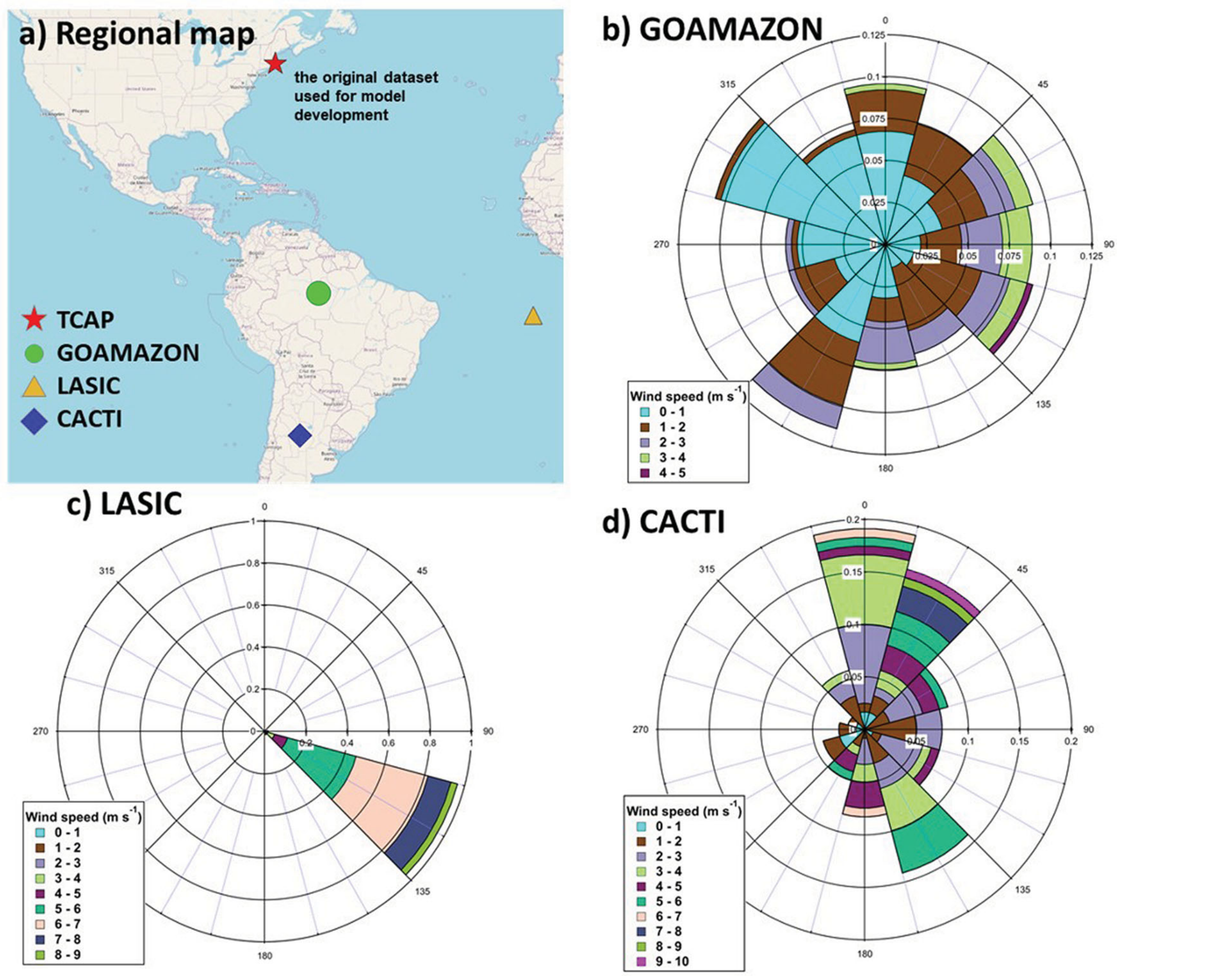

Figure 2. Locations of the investigated DOE ARM campaigns (panel (a)) and wind roses (panels (b–d)) illustrating the wind directions during the campaigns. In panels (b–d), different color bands represent different range of wind speeds and the length of each segment represents the relative frequency of wind from that direction. See the online version for a colorized figure.

Datasets used for model evaluation

The datasets studied in this work are from three US DOE ARM field campaigns: GOAMAZON, LASIC, and CACTI. As shown in Figure 2a, all campaigns took place in the southern hemisphere: GOAMAZON occurred downwind of the city of Manaus in Brazil (June–July 2014); LASIC was conducted on Ascension Island in the South Atlantic (January 2017); and CACTI was sited in a mountainous area of Argentina (December 2018). Wind analysis of the sites (Figures 2b–d) reveals that the wind direction varied widely at GOAMAZON but was only from southeast at LASIC. The consistency of wind patterns at LASIC is likely related to the prevailing trade winds near the equator. At CACTI, the winds from north and southeast had relatively higher frequencies. Among the three sites, LASIC had the greatest wind speeds (5.9 ± 1.1 m s^{-1}), followed by CACTI (3.1 ± 1.8 m s^{-1}) and GOAMAZON (1.2 ± 0.9 m s^{-1}). These wind patterns allow us to infer how the variability of aerosol sources affects the performance of our model in different locations.

We also probed the emission sources using backward trajectories analysis from NOAA's HYSPLIT4 model (Stein et al. 2015). During LASIC (Figure S1a), the trajectories originated in the South Atlantic Ocean to Ascension Island from a southeasterly direction, which is consistent with the wind rose plot in Figure 2c. During CACTI, the air mass trajectories' origins differed in time and space. In the first week of the study (Figure S1b), the air mass trajectories origin was from the South Pacific Ocean, likely transporting marine aerosols (e.g., sea spray) to the area of study. Later in the study (Figure S1c), there appears to be a larger contribution of terrestrial aerosols when the trajectories originated from northeast. Interestingly, although the backward trajectories at GOAMAZON are mostly from southeast, the pathway of aerosols between 06/24/14 and 07/24/14 (Figure S2b) would potentially bring many marine aerosols to the study area. However, in the other days, trajectories mainly originated from over land than over the ocean (Figures S2a and c).

We selected these campaigns for our analysis for the following reasons. First, these studies used similar instrumentation (both among each other and compared to the TCAP training data for our SVM model) to characterize the aerosols, which may constrain the influence of measurement uncertainties in model performance evaluation. For example, all studies utilized SP2 for BC mass, filter-based absorption photometers for multi-wavelength B_{abs}, nephelometers for multi-wavelength B_{scat}, and at least an SMPS for particle size distributions. Even though the filter-based instruments may be prone to biases (even after the application of correction algorithms), we assume that these biases will be similar across the campaigns. Second, these campaigns were conducted at different observational sites representing different atmospheric environments than TCAP, which occurred near Cape Cod, Massachusetts, USA (July–August 2012). The variation in aerosol sources and properties among these three additional campaigns allows us to probe the generalizability of the models. Third, a relatively large number of time-series observations were reported for these campaigns, which is necessary to capture the temporal variations in MAC at the sites.

Results and discussion

Overview of the aerosol properties

We summarize relevant observations from the three campaigns in Table 1. We report the results using 4-h averages, in order to dampen both the temporal variability and measurement uncertainty within the data. For all studies, the ambient BC mass concentration was roughly 0.11 μg m^{-3} yet with a relatively large standard deviation during each campaign (nearly 70%; see Table 1). Similarly, the observed B_{abs} at 870 nm, as corrected by the correction scheme reported in Bond, Anderson, and Campbell (1999) (hereafter referred to as B1999), was roughly 1 Mm^{-1} across the three campaigns, although the temporal variability was greater during both GOAMAZON and CACTI (roughly 60–70%) than during LASIC (roughly 40%). Given that we are considering 4-h-averaged data, we expect that this variability is driven more by temporal variations than measurement uncertainty. The application of an alternative correction method for the filter-based absorption measurements (Li, McMeeking, and May (2020); hereafter, L2020) reduced the corrected B_{abs} values by roughly a factor of two compared to B1999, but the variability among the studies remains similar. This comparison reinforces prior studies suggesting that systematic biases exist among different correction schemes for filter-based absorption photometers (Li, McMeeking, and May 2020; Davies et al. 2019; Saturno et al. 2017; Collaud Coen et al. 2010). This is perhaps unsurprising, because these algorithms were developed using different reference measures of B_{abs}, different aerosol types, and different input parameters; for example, B1999 was developed using laboratory aerosols and uses transmission through the filter (Tr) and B_{scat} as inputs to the correction, while L2020 was

Table 1. Average (standard deviation) of major meteorological parameters and aerosol properties measured at the campaigns, based on 4-h averages. MAC, B_{abs}, and SSA are reported for 870 nm.

Dataset	GOAMAZON	GOAMAZON (subset[a])	LASIC	CACTI	TCAP (training data)
Location (latitude and longitude)	−3.21°, −60.70°	−3.21°, −60.70°	−7.97°, −14.35°	−32.13°, −64.73°	42.03°, −70.05°
Collection period (MM/DD/YY)	06/15/14–07/31/14	Excluding 06/24/14–07/24/14	01/14/17–01/23/17	12/01/18–12/20/18	07/16/12–08/15/12
Number of data	225	81	60	120	583
Temperature (°C)	26.62 (2.90)	26.50 (2.93)	23.94 (1.14)	18.60 (4.47)	23.45 (2.90)
Relative humidity (%)	88 (11)	88 (11)	87 (6)	71 (17)	86 (12)
Wind direction (°)	174 (106)	186 (105)	119 (7)	139 (110)	199 (79)
Wind speed (m s^{-1})	1.17 (0.88)	1.08 (0.79)	5.94 (1.14)	3.07 (1.78)	3.69 (1.86)
MAC_{meas} (L2020, m^2 g^{-1})	6.49 (3.18)	3.53 (2.46)	/	2.94 (1.03)	3.87 (1.92)
MAC_{meas} (B1999, m^2 g^{-1})	13.89 (6.24)	6.94 (1.38)	7.92 (0.71)	7.37 (2.11)	7.81 (4.11)
B_{abs} (L2020, Mm^{-1})	0.49 (0.35)	0.49 (0.30)	/	0.31 (0.17)	0.32 (0.28)
B_{abs} (B1999, Mm^{-1})	1.12 (0.78)	1.14 (0.74)	0.97 (0.37)	0.80 (0.49)	0.80 (0.68)
AAE	1.33 (0.24)	1.35 (0.24)	0.93 (0.06)	1.33 (0.30)	1.57 (0.66)
SAE	0.95 (0.21)	0.89 (0.23)	0.64 (0.10)	1.17 (0.64)	1.38 (0.45)
SSA (L2020)	0.96 (0.02)	0.96 (0.02)	/	0.96 (0.03)	0.97 (0.02)
SSA (B1999)	0.93 (0.03)	0.93 (0.02)	0.94 (0.03)	0.92 (0.02)	0.93 (0.04)
SP2 M_{BC} (μg m^{-3})	0.10 (0.07)	0.14 (0.08)	0.12 (0.05)	0.11 (0.08)	0.10 (0.07)
shell mass/BC core mass[b]	29.1 (17.2)	16.0 (9.0)	1.5 (4.5)	24.1 (23.0)	–
SP2 D_{median} (nm)	97 (4)	98 (5)	155 (4)	86 (5)	–
SMPS D_{median} (nm)	50 (11)	49 (11)	119 (16)	56 (24)	68 (20)

[a]The subset of GOAMAZON excludes the observations from 6/24/2014 to 7/24/2014 when MAC_{BC} values showed elevated levels (Figure 4a). The substantial increase in MAC_{BC} values may be associated with the absorption enhancement of BC by mixing with organic and inorganic coatings or the presence of larger absorbing aerosols.
[b]Shell masses are estimated using Equation (4).

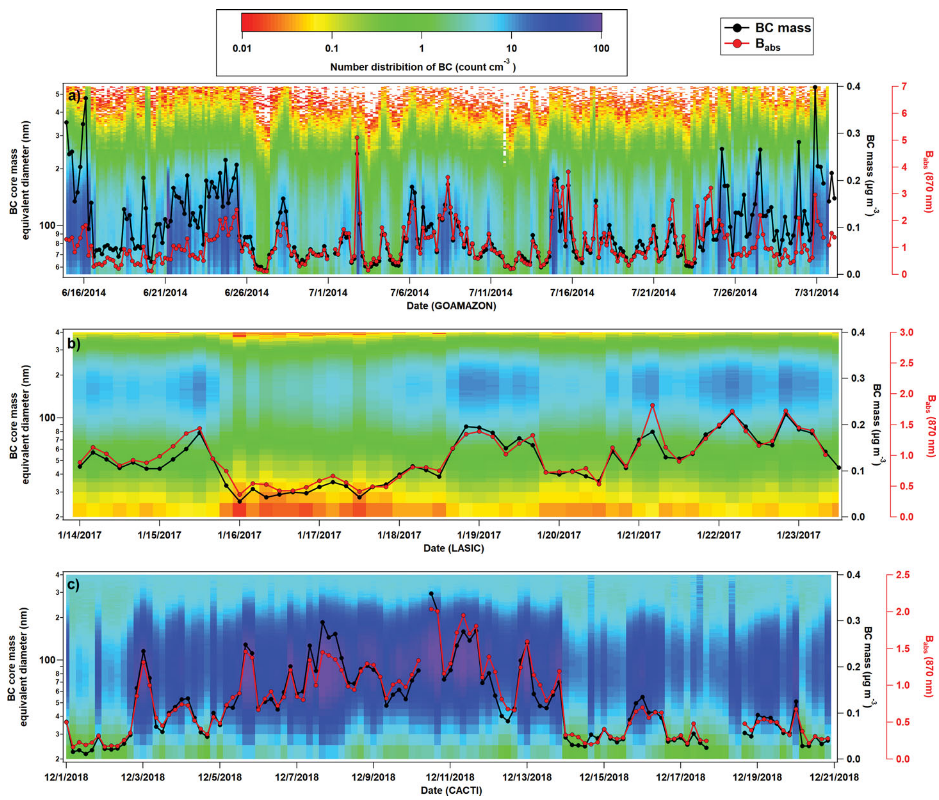

Figure 3. Time series (MM/DD/YYYY, based on 4-h averages) of BC number size distribution overlapped with the mass concentration of BC and B_{abs} at 870 nm (corrected by the B1999 correction). Note that the x axis of BC core diameter in panel (a) starts at 55 nm (the other two panels start at 15 nm), based on the data provided within the DOE ARM Data Discovery website. The right axis of B_{abs} is scaled differently in the three panels. See the online version for a colorized figure.

developed using ambient aerosols and uses not only Tr and B_{scat} but also SSA and AAE as inputs.

Nevertheless, we use these measurements of BC mass and B_{abs} (B1999 correction) to calculate the measured values of MAC (MAC_{meas}) at 870 nm, with average values ranging from ~7.5 m^2 g^{-1} (LASIC and CACTI) to 13.9 m^2 g^{-1} (GOAMAZON). However, using the L2020 correction reduces the MAC_{meas} values to 6.5 m^2 g^{-1} for GOAMAZON and 3 m^2 g^{-1} for CACTI; applying the L2020 correction to LASIC was not possible, because neither raw transmittance nor attenuation recorded by the filter-based absorption photometer was available on the DOE ARM Data Discovery site for that campaign. In the following sections, we use B1999 to obtain the results of MAC_{meas}, AAE, and SSA, unless otherwise specified. Similarly, we used the SVM model tailored for the input variables of B1999-corrected B_{abs} to derive MAC_{SVM}. Finally, we note that the mean of a ratio is not necessarily equal to the ratio of the mean values of two distributions, which is why the mean MAC values in Table 1 differ from B_{abs} divided by M_{BC}.

Figure 3 illustrates the time series of BC particle number distributions as a function of BC core diameter (left y axis) measured by the SP2. Comparing the number distributions between the sites, we observe that GOAMAZON and CACTI are dominated by BC particles between 55 and 200 nm, and CACTI appears to have more large BC particles (i.e., >250 nm) than GOAMAZON. At the LASIC site, the number concentration of BC particles is smaller than that from the other two campaigns, and the particles of 100–200 nm constituted the major component of the total BC concentrations. The relatively small variation in the BC size distribution at LASIC may be explained by the small changing of wind direction at the site (Figure 2c).

In each panel of Figure 3, the black and red curves present the temporal changes in BC mass concentration and B_{abs} at 870 nm, respectively. Interestingly, we note that from 6/24/2014 to 7/24/2014 during the GOAMAZON campaign, SP2 detected fewer BC particles smaller than 200 nm compared to the other days, resulting in roughly 50% lower mass concentrations of BC particles. However, the B_{abs} measurements during this period tended to be similar or slightly greater than the other times. This abnormal period leads to an elevated value of MAC_{meas} in Figure 4a. Excluding this window, MAC_{meas} at 870 nm decreases from 13.89 to 6.94 m^2 g^{-1} (B1999) and from 6.49 to

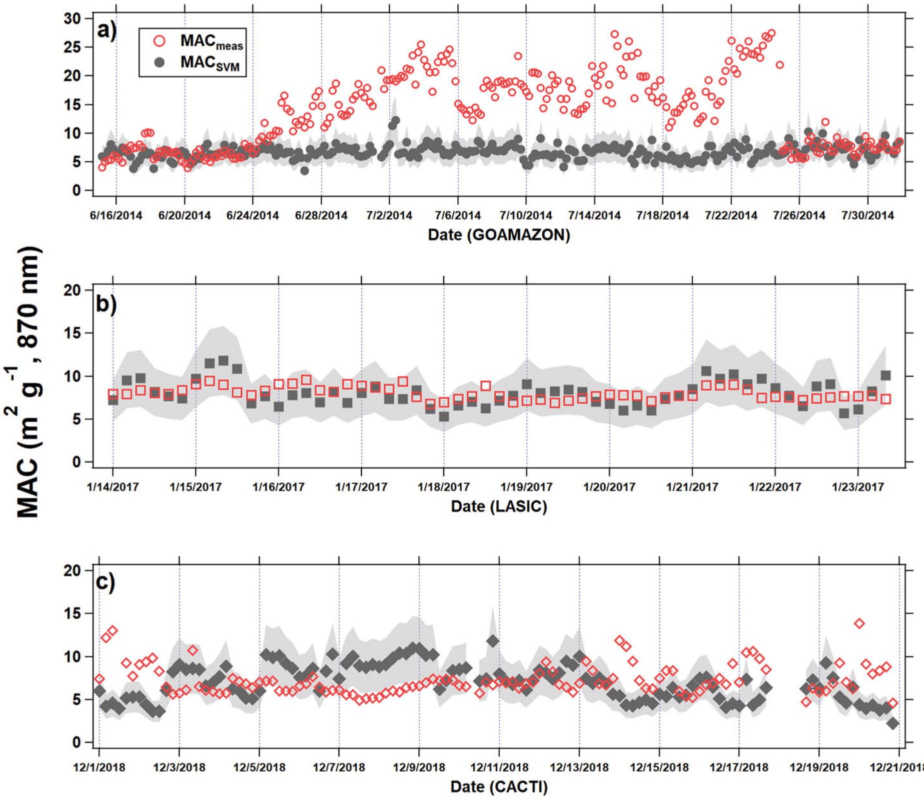

Figure 4. Time-series (MM/DD/YYYY) of MAC_{meas} and MAC_{SVM} at 870 nm obtained from the three campaigns. The shaded area represent a 34% prediction uncertainty of the SVM model reported in Li and May (2020a). Note that the y axis in panels (a) differ from those in (b) and (c) due to the enhanced MAC_{meas} values between 06/24/14 and 07/24/14 at GOAMAZON. See the online version for a colorized figure.

3.53 $m^2\ g^{-1}$ (L2020). We discuss this further in the section "BC coating and its influence on model accuracy." During the LASIC and CACTI campaigns, the measured BC mass and B_{abs} exhibited a similar pattern over time, resulting in the averaged MAC_{BC} of 7.92 and 7.37 $m^2\ g^{-1}$ (B1999), respectively. We observed a relatively small temporal variation in MAC_{BC} during LASIC (roughly 10%), presumably because the wind direction and aerosol sources were very consistent (Figure 2c and Figure S1a).

Variability of MAC obtained by different methods

We next compare time series of MAC_{SVM} to time series of MAC derived from observations (i.e., MAC_{meas}) using B1999 for GOAMAZON (Figure 4a), LASIC (Figure 4b), and CACTI (Figure 4c). Generally, our machine learning model performs well. With the exception of the period within GOAMAZON discussed previously and for some of the periods within CACTI, MAC_{SVM} agrees with MAC_{meas} within the model's uncertainty (shaded region in Figure 4). Moreover, the SVM model generally captures the temporal variability in MAC_{meas} (ranging from 10% to 70%, depending on the campaign); temporal variations cannot be captured by the standard assumption of roughly 4.5 $m^2\ g^{-1}$ at 870 nm. The reduced performance of the SVM model during CACTI is not surprising considering the variability of wind direction and likely contribution of different sources to BC particles. For example, wind erosion of dust due to local convective storms (Schumacher et al. 2021) and the resulting large airborne particles (SAE < 0.5) may partially explain the degradation of the SVM model, as we discuss in May and Li (2022); transport of mineral dust or sea spray aerosols to the observation site during GOAMAZON may also be a plausible explanation for poor agreement during the 6/24/2014 to 7/24/2014 period.

We expand upon these comparisons in Figure 5, which presents box-and-whisker plots of MAC_{meas} (using both B1999 and L2020, where possible) as well as our predictions: MAC_{SVM}, MAC_{RDG}, $MAC_{Mie,ext}$, $MAC_{Mie,int}$, and $MAC_{empirical}$ for all three campaigns. GOAMAZON results include the full dataset (Figure 5a) as well as the subset discussed previously (Figure 5b). We also provide the "standard" MAC_{BC} at 870 nm based on Bond and Bergstrom (2006) inferred using $AAE_{BC} = 1$, that is, 4.74 $m^2\ g^{-1}$ (dashed

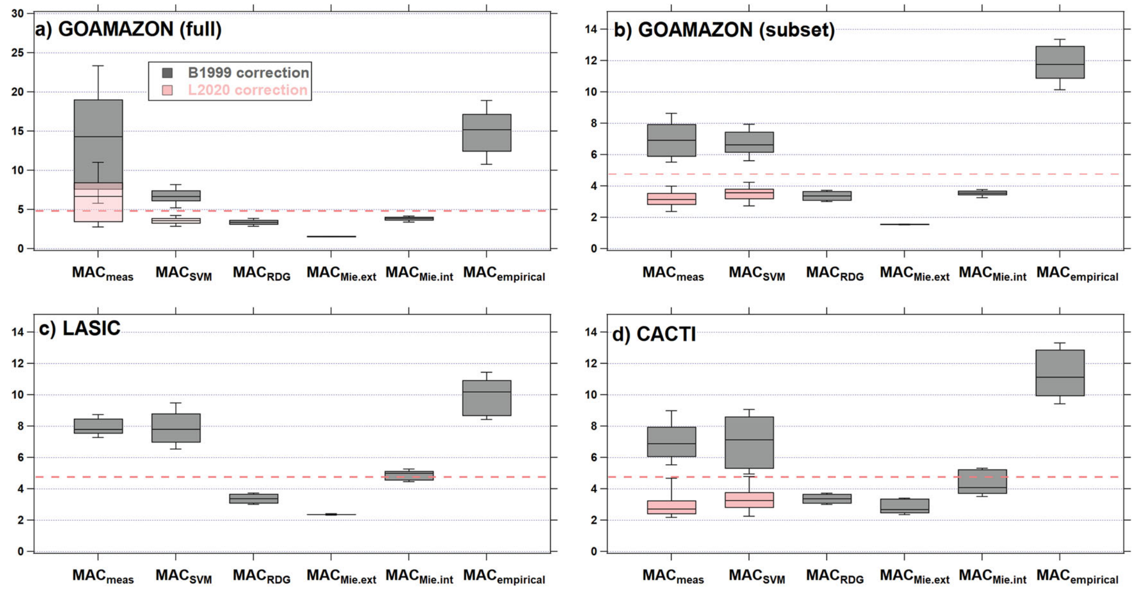

Figure 5. Comparison between MAC_{meas} and predicted MAC by different methods. For the studies of GOAMAZON and CACTI, both B1999 and L2020 corrections were used to derive the filter-based B_{abs} and MAC_{meas}. Similarly, the corresponding two versions of SVM model were applied when predicting MAC_{SVM}. The boxplots in panels (a) and (b) are derived using all GOAMAZON data and a subset excluding 06/24/14–07/24/14, respectively. The dashed red line represents MAC of $4.74\,m^2\ g^{-1}$ (the "standard assumption" with AAE = 1). Note that the y axis range is different in panel (a). See the online version for a colorized figure.

horizontal lines). The predicted MAC_{BC} values from different models are not consistent. For example, the empirical model always produces the highest predictions ($MAC_{empirical}$), leading to roughly 30% over-prediction compared to MAC_{meas} in Figures 5b–d, which suggests that some BC particles may not be internally mixed. Conversely, Mie theory with an assumption of external mixing ($MAC_{Mie,ext}$) results in the lowest values: roughly $2\,m^2\ g^{-1}$ for all datasets. Hence, $MAC_{Mie.int}$ values are greater than $MAC_{Mie.ext}$ by factors up to 2, resulting in good agreement compared to the "standard" MAC_{BC} for all three campaigns. As described above, the raw modeled MAC_{RDG} was adjusted by a factor of 0.9 to 1.3 as recommended in Liu et al. (2020) to account for uncertainties. With the exception of the full GOAMAZON dataset (which is arguably bimodal with central values around $5\,m^2\ g^{-1}$ and $15\,m^2\ g^{-1}$, as in Figure 4a), Figure 5 suggests that the standard assumption cannot represent any of these data.

We quantify the performance of each method for estimating MAC_{BC} in Table 2 by calculating the difference between the mean predicted value and MAC_{meas} as well as a *t*-test comparing the two means. Based on this analysis, our SVM model performs well; with the exception of the full GOAMAZON dataset, the difference between the mean values of MAC_{SVM} and MAC_{meas} are generally small and not statistically significant. Conversely, the performance of the other models is variable across sites. For example, the RDG-FA approximation (MAC_{RDG}) and core-shell Mie theory ($MAC_{Mie.int}$) generally agree with GOAMAZON subset corrected by L2020 in Figure 5b and CACTI in Figure 5d, but they under-predict MAC_{meas} for LASIC (Figure 5c). Notably, the variability of MAC_{meas} observed during the three campaigns (Table 1 and Figure 4) cannot be captured by the RDG-FA theory, because it does not take into account the temporal variability, even with the simple adjustment that we have applied. Similarly, the Mie theory models and the empirical model rely on the BC mass measured by the SP2, so they are not applicable for the locations without the deployment of an SP2; the lack of an SP2 appears to be common in many long-term observational sites (e.g., the US DOE ARM fixed-location observatories and many sites within the US National Oceanic and Atmospheric Administration Global Monitoring Laboratory Federated Aerosol Network).

Table 2. The differences between the means of the predicted MAC_{BC} values and MAC_{meas}. The underlined and italicized values in the table indicate *t*-tests yielding *p*-value > 0.05 (i.e., no statistical significance between prediction and observation).

	SVM	RDG	Mie.ext	Mie.int	Empirical
GOAMAZON (full; L2020)	−2.92	−3.01	−4.95	−2.68	8.37
GOAMAZON (full; B1999)	−7.19	−11.17	−12.39	−10.12	0.9
GOAMAZON (subset; L2020)	0.26	*0.14*	−1.62	0.35	8.57
GOAMAZON (subset; B1999)	*-0.30*	−3.87	−5.54	−3.57	4.66
LASIC (B1999)	*0.003*	−4.65	−5.64	−3.15	1.93
CACTI (L2020)	*0.34*	*0.18*	*-0.28*	0.98	7.95
CACTI (B1999)	*-0.23*	−3.91	−4.42	−2.92	3.95

On the other hand, our model is built on real-time measurements of aerosols common to these sites and does not appear to be hindered by the fact that it does not explicitly represent the underlying physics of aerosol light absorption (e.g., it is agnostic to aerosol mixing state). Thus, it has the potential to be generalizable across different atmospheric environments.

The variability caused by different correction algorithms applied to B_{abs} cannot be ignored when deriving MAC_{meas}. As a result, an efficient MAC_{BC} prediction model should take into account the uncertainty of B_{abs} and adjust its parameters. As seen in Figure 5, only the SVM model can yield consistent agreement with MAC_{meas} when changing from B1999 to L2020, especially for the GOAMAZON subset (panel (b)) and CACTI (panel (d)). Interestingly, the RDG and Mie models tend to agree better with the MAC_{meas} using L2020, but the empirical model agrees better with MAC_{meas} using B1999. In Li, McMeeking, and May (2020), we developed our algorithm for filter-based photometer corrections using the B_{abs} observations from a photoacoustic instrument, so this version of the SVM model will be also suitable for photoacoustic measurements. Similar to the lower MAC_{meas} values observed when applying the L2020 correction for photoacoustic measurements, Wei et al. (2020) assessed the MAC_{BC} values derived by different techniques in the literature and found that photoacoustic spectroscopy data exhibit a 20% lower MAC_{BC} than filter-based studies.

BC coating and its influence on model accuracy

As we have stated previously, the enhancement of light absorption due to a lensing effect could bias the MAC_{BC} results, because the coating layer can act as a focusing lens to enhance the incoming light to the BC cores. Thus, it is important to investigate how the proposed MAC_{BC} models perform when BC particles are coated by other materials at various thicknesses. For this purpose, we evaluate the relationship between BC coating state and the accuracy of different models in this section, with the inherent assumption that all BC is internally mixed with other aerosol species. Using the measurements from both SP2 and SMPS during the three campaigns, we calculated E_{abs} as the ratio of B_{abs} (core-shell) to B_{abs} (uncoated), both obtained from the appropriate Mie theory calculation. To estimate the ensemble-average relative coating thickness, we use the term $Ratio_{mass}$ (Cappa et al. 2019; Wu et al. 2018; Liu et al. 2015), which is defined as the coating-to-core mass ratio of BC-containing

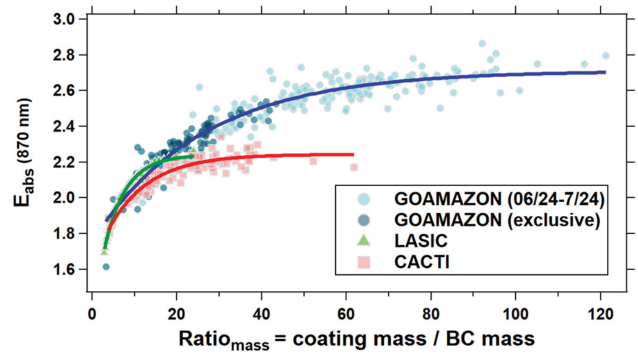

Figure 6. Variation in E_{abs} (870 nm) as a function of $Ratio_{mass}$. The lines (estimated by exponential functions) are used only to guide the eye. GOAMAZON (exclusive) refers to the subset of the data discussed elsewhere. See the online version for a colorized figure.

particles (i.e., $mass_{coating}$ in Equation (3) divided by SP2-derived BC mass). It is worth noting that the estimated E_{abs} from this work may differ from the measured E_{abs} in literature (using a thermodenuder to remove the coatings of BC particles). Fierce et al. (2020) reported the overestimate of E_{abs} by core-shell Mie theory and found that the deviation could be due to the inadequate consideration of heterogeneity among BC-containing particles and the simplification of core-shell approximation.

In general, we find that E_{abs} increases with increasing $Ratio_{mass}$, but the relationships vary across campaigns (Figure 6). For the LASIC and CACTI campaigns, the growth of E_{abs} is steep in the $Ratio_{mass}$ range of $2-15$, and then plateaus at $E_{abs} \approx 2.2$ beyond $Ratio_{mass} \approx 20$. On the other hand, the GOAMAZON campaign has broader ranges of both E_{abs} and $Ratio_{mass}$, resulting in a later transition to a plateau at roughly Eabs $\approx$ 2.7 and $Ratio_{mass} \approx 60$. Figure 6 also shows that the extremely high MAC values between 6/24 and 7/24 at GOAMAZON are associated with greater values of E_{abs} and $Ratio_{mass}$ (light blue markers). Although we do not have a full explanation for this period of GOAMAZON, our results suggest that either substantial coating materials condensed upon BC-containing particles, resulting in an enhancement effect of MAC_{BC}, or the BC was only partially internally mixed; that is, it is also externally mixed with other absorbing material such as tar-like brown carbon or mineral dust. However, our SVM model was unequivocally the most accurate model in predicting MAC_{BC} for laboratory-generated biomass burning emissions in Li and May (2020a), so the extent to which tar-like brown carbon influenced these results during GOAMAZON may be small.

Our observation in Figure 6 is consistent with previously published simulations and measurements of

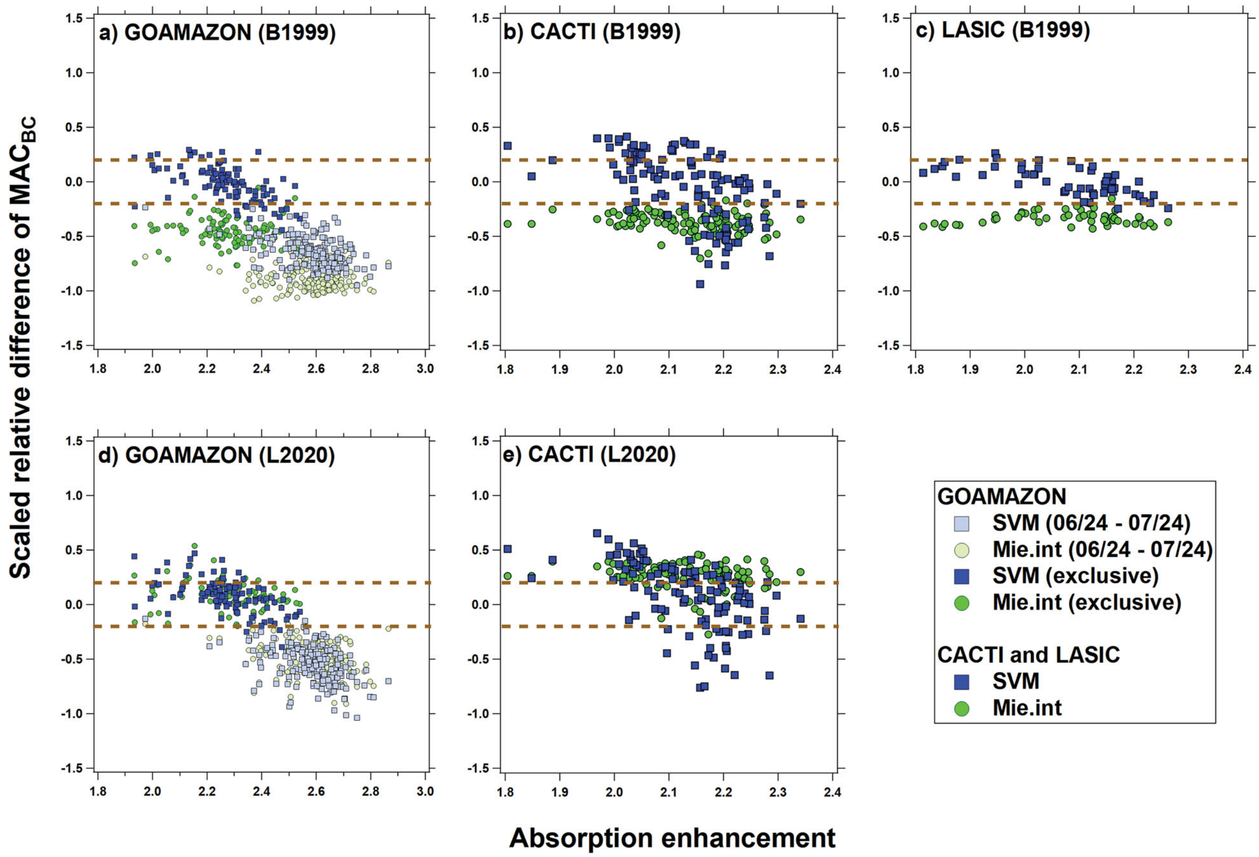

Figure 7. MAC_{BC} model prediction accuracy as a function of $Ratio_{mass}$. The dashed horizontal lines encapsulate the region of points where predictions agree with the measured value within ±33%, and the dashed vertical line represents the upper bound of $Ratio_{mass}$ in the TCAP training data. The GOAMAZON dataset are separated into the time period between 6/24/14 and 7/24/14 and the remainder of the campaign (denoted as "exclusive" in the legend). Note that the x axis of three campaigns is different. See the online version for a colorized figure.

$Ratio_{mass}$-dependent E_{abs} for internally mixed BC particles. Wu et al. (2018) described the relationship between $Ratio_{mass}$ and E_{abs} as a multistage process which is dependent on particle morphologies and sizes (Start: $E_{abs} < 1.2$ and $Ratio_{mass} < 1$; Rise:: $1.2 < E_{abs} < 2.55$ and $1 < Ratio_{mass} < \sim 200$; Stable: $E_{abs} > 2.55$ and $Ratio_{mass} > 200$). By comparing to laboratory and field measurements, they found that E_{abs} of BC particles that have undergone atmospheric aging varied from 1.8 to 2.7, which is in agreement with our results at the three ambient observational sites. In contrast, if the ambient environment has continuous and fresh emission of BC particles, the magnitude of E_{abs} is typically small (Cappa et al. 2012).

We next investigate how BC coatings influence the performance of different predictive MAC_{BC} models. Here, we focus on the results of MAC_{SVM} and $MAC_{Mie,int}$, because they are in good agreement with MAC_{meas} for all three campaigns in Figure 5. Moreover, because of the focus on coated BC particles, the inclusion of either RDG-FA or Mie theory for external mixtures is inappropriate. In our analysis, we assess the accuracy of the predicted MAC_{BC} using the EPA-recommended scaled relative difference (SRD) between MAC_{model} and MAC_{meas} (Gorham et al. 2021; Hyslop and White 2009):

$$SRD = \frac{(MAC_{model} - MAC_{true})/\sqrt{2}}{(MAC_{model} + MAC_{true})/2} \tag{7}$$

The SRD normalizes the difference between two values by their mean and includes a term of $\sqrt{2}$ to account for uncertainty in the values.

The SRD results of the SVM and Core-shell Mie models are shown against $Ratio_{mass}$ in Figure 7. Overall, a negative trend (i.e., a proportional bias) exists between SRD and $Ratio_{mass}$ for our SVM model. When $Ratio_{mass}$ is greater than roughly 30, the SVM model underestimates the measured value by roughly a factor of two (SRD ≈ -0.5); however, when $Ratio_{mass}$ is less than roughly 25, the majority of the SVM results fall within the SRD = ±0.2, which corresponds to roughly ±33% difference between the values. This relatively good agreement at the lower values of $Ratio_{mass}$ is expected, because these are more

Table 3. A comparison of MAC_{BC} prediction models and their performance for different atmospheric BC particles.

Approach	Required measurements	Key assumptions	Accuracy	Major limitations
Field observations	• BC mass concentration • B_{abs} at desired λ	• N/a	High	• Observations may not exist at all locations
Standard assumption	• N/a	• Fresh BC particles	Variable	• The value may not be applicable for aged BC particles • It cannot capture spatiotemporal variability
RDG-FA	• N/a	• Fractal aggregate morphology • BC density • BC complex refractive index	Variable	• Aggregates may become more compact in the atmosphere • It cannot capture spatiotemporal variability
Mie theory (external mixing)	• BC mass concentration • BC size distribution	• Spherical particles • BC is externally mixed • BC density • BC complex refractive index	Generally underpredicts	• Exact morphology and mixing state may be unknown • Assumptions of aerosol microphysical parameters are required
Mie theory (core-shell)	• BC mass concentration • BC size distribution • Total particle size distribution	• Spherical particles • BC is internally mixed • BC density • BC complex refractive index • Coating material density • Coating material complex refractive index	Variable	• Exact morphology and mixing state may be unknown • Assumptions of aerosol microphysical parameters are required
SVM	• B_{abs} at multiple λ • B_{scat} at multiple λ • Total particle size distribution	• N/a	Relatively high under certain conditions	• Degradation to performance when aerosols are different from the training data
Empirical	• BC mass concentration • Total particle mass concentration	• BC is internally mixed	Generally overpredicts	• Exact mixing state may be unknown

representative of the TCAP training dataset (mean = 8.18 ± 3.78; range: [0.67, 19.96]). We did not calculate E_{abs} for TCAP because SP2 size distributions are unavailable through the US DOE ARM Data Discovery; however, based on the empirical relationship from Chakrabarty and Heinson (2018) for internal mixtures: $E_{abs} = 1.0 \cdot (Ratio_{mass})^{0.33}$, an estimated mean value of E_{abs} for TCAP is 2.00 (with a range of 0.88–2.69) which is more similar to the E_{abs} values observed at CACTI and LASIC (Figure 6). Because both CACTI and LASIC have lower overall $Ratio_{mass}$ and E_{abs}, similar to the training data, our SVM model generally works well for the entirety of these datasets. Consequently, if the ambient environment has BC particles with mild to moderate coating thickness, we infer that our SVM model will work fairly well to estimate MAC_{BC}; otherwise, if the BC particles are thickly coated, MAC_{SVM} is lower than measured values, likely because the model is extrapolating away from the range constrained by the training data.

In contrast, no obvious trend exists between SRD and $Ratio_{mass}$ for the core-shell Mie model, but systematic biases are present. For example, if B1999 is used to correct B_{abs} data, $MAC_{Mie.int}$ is biased low with a mean SRD of roughly −0.3 across the three campaigns (Figures 7a–c), suggesting that our assumption that the coating material is non-absorbing is incorrect. However, when we use L2020, the predictions from $MAC_{Mie.int}$ are more similar to MAC_{SVM}, and in the case of the CACTI data, $MAC_{Mie.int}$ is biased slightly high; this latter observation may suggest that not all of the non-BC material is internally mixed with BC.

Practical assessment of the models

Our analysis of BC particles during field observations suggests that there is no perfect approach to predict MAC_{BC} with good performance under all environmental conditions (summarized in Table 3). However, given our intention to develop a simple yet relatively robust model to estimate atmospheric MAC_{BC} values, the results reported in the present work and our other work (May and Li 2022; Li and May 2020a) suggest that our SVM model has potential. Although it is not a physics-based model, it is physics-inspired in that it emulates light scattering theory by using proxies for aerosol size distributions and aerosol composition. Moreover, while it is agnostic to properties specific to

BC (e.g., complex refractive index, mixing state), it can capture most time-series trends. Therefore, our SVM model may represent a useful approach toward converting between BC light absorption and BC mass concentrations—which has implications for the evaluation of chemistry-climate model predictions of BC radiative forcing.

The assumptions related to aerosol microphysics (e.g., volume ratio of shell to core, refractive indices of BC and coating material, and particle densities) play important roles for theoretical models. For example, the calculated MAC_{BC} values from both the RDG-FA approximation and Mie theory models are sensitive to the refractive indices of particles. Assuming a different BC complex refractive index, for example, 1.8 + 1.4i at 870 nm from Forestieri et al. (2018), we calculate $MAC_{RDG} = 5.03\,m^2\,g^{-1}$, which is 60% greater than our original estimation of MAC ($3.06\,m^2\,g^{-1}$). This new MAC_{RDG} agrees better with the value of $4.74\,m^2\,g^{-1}$ extrapolated from the recommended value from Bond and Bergstrom (2006) assuming AAE = 1. Similarly, the underestimation of MAC_{BC} by Mie theory for external mixing can be improved by increasing the imaginary refractive index of BC. In the core-shell configuration of Mie theory, the complex refractive index of the coating material is another free parameter, which has been found to result in greater uncertainty in E_{abs} and MAC_{BC} than the variation in the BC's refractive index (Zhang et al. 2018).

In ambient air, the exact mixing states and morphologies may be unknown. For simplicity, we only considered theoretical frameworks for fresh fractal aggregates, externally mixed particles, and concentric core-shell internally mixed particles. However, the geometry of partially coated BC (i.e., inhomogeneous internal mixtures) is likely (Wang et al. 2021; Fierce et al. 2016, 2020; Wu et al. 2018). There have been some theoretical studies that have explored the absorbing properties of partially coated BC using complex models with many free parameters (Zhang et al. 2018; He et al. 2015), but the applicability of these models to real-world observations is limited by a lack of empirical constraints on these parameters.

Conversely, our SVM model does not require any assumptions on particle mixing states and morphologies. However, its main limitation is the training data. The model was trained using input values from TCAP, and while some input values from GOAMAZON, CACTI, and LASIC were similar to the training data, others were not. For example, during LASIC, the mean AAE and SAE were 0.93 ± 0.06 and 0.64 ± 0.10, respectively, while in the training data, these values were 1.57 ± 0.66 and 1.38 ± 0.45. Thus, our SVM model is effectively extrapolating for the majority of the LASIC data. Nevertheless, our SVM model appears to be generalizable, in that it tends to perform well even for scenarios divergent from the training data. Consequently, although our SVM model does not require the input of particle mixing state during its implementation, some knowledge of the mixing state is still required to either verify if the model is used in the right regime or to train the model on other regimes.

However, one factor influencing the evaluation of all models is measurement uncertainty, especially for low values of B_{abs}. Based on Ogren et al. (2017), we infer an uncertainty of roughly 25% when $B_{abs} = 1\,Mm^{-1}$ using B1999; in Li, McMeeking, and May (2020), we estimate an uncertainty of 10% for our algorithm. Moreover, May et al. (2014) estimated an uncertainty of roughly 22% for SP2 measurements of BC mass concentrations. Therefore, propagating this uncertainty via quadrature, we obtain estimates in MAC_{meas} of roughly 24% (L2020) and roughly 34% (B1999). These uncertainties are similar to the relative standard deviations presented in Table 1, for example, for both B1999 and L2020, the relative standard deviation is roughly 50% for both GOAMAZON and TCAP, and it is roughly 35% for CACTI. However, given our 4-h averaging time used in our data analysis, we expect that the effect of measurement uncertainty is largely dampened, which is supported by the clear temporal trends for all datasets in Figure 3. Thus, while measurement uncertainty cannot be completely discounted, we argue that it plays a small role in our analysis and interpretation.

Conclusions

We have used theoretical (both RDG-FA approximation and Mie theory), empirical (Chakrabarty and Heinson 2018), and machine learning (Li and May 2020a) models to estimate MAC_{BC} of black carbon particles at 870 nm using inputs from different observational sites. The comparison between the modeled and measured response of MAC_{BC} suggests that the SVM model is more accurate across these different environments than the other models, as the SVM model yields consistently good agreement with MAC_{meas} over the three sites. Moreover, the derived MAC_{meas} values vary by a factor of 2 when the correction algorithm applied to filter-based B_{abs} data changes (B1999 vs. L2020); only the SVM model can adapt to these differences, as we have built different bias corrections into a data preprocessing step for this model. Importantly, most of these models capture the temporal variability in MAC_{meas}—ranging from 10% to 70% (Table 1)—which the standard assumption (a constant value with ± 20% uncertainty) simply cannot do.

Generally, the accuracy of the theoretical and empirical models that we have considered is not as good as our SVM model (Figure 5; Table 2). More complex and sophisticated optical models, such as multiple-sphere T-matrix (MSTM) and generalized multi-particle Mie (GMM), may provide MAC_{BC} closer to reality (Wei et al. 2020). However, these models are typically time-consuming and rarely applied to long-term BC monitoring. Liu et al. (2017) estimated that the computational time of the MSTM method for single BC aggregates comprised of 200 monomers is on the order of 10 s, using "a single node with 24 64-bit 2.5 GHz processors." Conversely, our SVM model takes less than 1 min to predict 3000 MAC_{BC} values for the dataset provided in Li and May (2020b) using a laptop computer. One caveat is that when the SVM model performs calculations using observations outside of the data on which it was trained (e.g., $Ratio_{mass} > 20$), its predictions may become unreliable, so future work may be needed to train the SVM model using a set of aerosol properties from a more diverse set of field observations.

Funding

This work was funded by the Atmospheric Chemistry, Carbon Cycle, & Climate program within the National Oceanic and Atmospheric Administration's Climate Program Office through award NA16OAR4310109. The ambient data at the TCAP, CACTI, LASIC, and GOAMAZON sites were obtained from the Atmospheric Radiation Measurement (ARM) user facility, a U.S. Department of Energy (DOE) Office of Science user facility managed by the Office of Biological and Environmental Research.

ORCID

Hanyang Li http://orcid.org/0000-0003-4465-5159
Andrew A. May http://orcid.org/0000-0001-7908-8815

Data availability statement

The DOE ARM field campaign data are available through https://www.archive.arm.gov/discovery/. The FIREX data are available from the project website https://www.esrl.noaa.gov/csl/projects/firex/firelab/.

Disclosure statement

No potential conflict of interest was reported by the author(s).

References

Adachi, K., S. H. Chung, and P. R. Buseck. 2010. Shapes of soot aerosol particles and implications for their effects on climate. *J. Geophys. Res.* 115 (D15):D15206. doi:10.1029/2009JD012868.

Backman, J., A. Virkkula, V. Vakkari, J. P. Beukes, P. G. Van Zyl, M. Josipovic, S. Piketh, P. Tiitta, K. Chiloane, T. Petäjä, et al. 2014. Differences in aerosol absorption Ångström exponents between correction algorithms for a particle soot absorption photometer measured on the South African Highveld. *Atmos. Meas. Tech.* 7 (12):4285–98. doi:10.5194/amt-7-4285-2014.

Bahadur, R., P. S. Praveen, Y. Xu, and V. Ramanathan. 2012. Solar absorption by elemental and brown carbon determined from spectral observations. *Proc. Natl. Acad. Sci. USA* 109 (43):17366–71. doi:10.1073/pnas.1205910109.

Bergstrom, R. W., P. B. Russell, and P. Hignett. 2002. Wavelength dependence of the absorption of black carbon particles: Predictions and results from the TARFOX Experiment and implications for the aerosol single scattering albedo. *J. Atmos. Sci.* 59 (3):567–77. doi:10.1175/1520-0469(2002)059<0567:WDOTAO>2.0.CO;2.

Bohren, C, and D. Huffman. 1983. *Absorption and scattering of light by small particles*. New York, NY: Wiley-Interscience.

Bond, T. C., T. L. Anderson, and D. Campbell. 1999. Calibration and intercomparison of filter-based measurements of visible light absorption by aerosols. *Aerosol. Sci. Technol.* 30 (6):582–600. doi:10.1080/027868299304435.

Bond, T. C, and R. W. Bergstrom. 2006. Light absorption by carbonaceous particles: An investigative review. *Aerosol Sci. Technol.* 40 (1):27–67. doi:10.1080/02786820500421521.

Bond, T. C., S. J. Doherty, D. W. Fahey, P. M. Forster, T. Berntsen, B. J. DeAngelo, M. G. Flanner, S. Ghan, B. Kärcher, D. Koch, et al. 2013. Bounding the role of black carbon in the climate system: A scientific assessment. *J. Geophys. Res. Atmos.* 118 (11):5380–552. doi:10.1002/jgrd.50171.

Bond, T. C., G. Habib, and R. W. Bergstrom. 2006. Limitations in the enhancement of visible light absorption due to mixing state. *J. Geophys. Res.* 111 (D20):D20211. doi:10.1029/2006JD007315.

Caponi, L., P. Formenti, D. Massabó, C. Di Biagio, M. Cazaunau, E. Pangui, S. Chevaillier, G. Landrot, M. O. Andreae, K. Kandler, et al. 2017. Spectral- and size-resolved mass absorption efficiency of mineral dust aerosols in the shortwave spectrum: A simulation chamber study. *Atmos. Chem. Phys.* 17 (11):7175–91. doi:10.5194/acp-17-7175-2017.

Cappa, C. D., K. R. Kolesar, X. Zhang, D. B. Atkinson, M. S. Pekour, R. A. Zaveri, A. Zelenyuk, and Q. Zhang. 2016. Understanding the optical properties of ambient sub- and supermicron particulate matter: Results from the CARES 2010 field study in northern California. *Atmos. Chem. Phys.* 16 (10):6511–35. doi:10.5194/acp-16-6511-2016.

Cappa, C. D., T. B. Onasch, P. Massoli, D. R. Worsnop, T. S. Bates, E. S. Cross, P. Davidovits, J. Hakala, K. L. Hayden, B. T. Jobson, et al. 2012. Radiative absorption enhancements due to the mixing state of atmospheric black carbon. *Science* 337 (6098):1078–81. doi:10.1126/science.1223447.

Cappa, C. D., X. Zhang, L. M. Russell, S. Collier, A. K. Y. Lee, C.-L. Chen, R. Betha, S. Chen, J. Liu, D. J. Price, et al. 2019. Light absorption by ambient black and brown carbon and its dependence on black carbon coating state for two California, USA, cities in winter and summer. *J. Geophys. Res. Atmos.* 124 (3):1550–77. doi:10.1029/2018JD029501.

Cazorla, A., R. Bahadur, K. J. Suski, J. F. Cahill, D. Chand, B. Schmid, V. Ramanathan, and K. A. Prather. 2013. Relating aerosol absorption due to soot, organic carbon, and dust to emission sources determined from in-situ chemical measurements. *Atmos. Chem. Phys.* 13 (18):9337–50. doi:10.5194/acp-13-9337-2013.

Chakrabarty, R. K, and W. R. Heinson. 2018. Scaling laws for light absorption enhancement due to nonrefractory coating of atmospheric black carbon aerosol. *Phys. Rev. Lett.* 121 (21):218701. doi:10.1103/PhysRevLett.121.218701.

Cho, C., S.-W. Kim, M. Lee, S. Lim, W. Fang, Ö. Gustafsson, A. Andersson, R. J. Park, and P. J. Sheridan. 2019. Observation-based estimates of the mass absorption cross-section of black and brown carbon and their contribution to aerosol light absorption in East Asia. *Atmos. Environ* 212:65–74. doi:10.1016/j.atmosenv.2019.05.024.

Collaud Coen, M., E. Weingartner, A. Apituley, D. Ceburnis, R. Fierz-Schmidhauser, H. Flentje, J. S. Henzing, S. G. Jennings, M. Moerman, A. Petzold, et al. 2010. Minimizing light absorption measurement artifacts of the aethalometer: Evaluation of five correction algorithms. *Atmos. Meas. Tech.* 3 (2):457–74. doi:10.5194/amt-3-457-2010.

Conrad, B. M, and M. R. Johnson. 2019. Mass absorption cross-section of flare-generated black carbon: Variability, predictive model, and implications. *Carbon N. Y* 149:760–71. doi:10.1016/j.carbon.2019.04.086.

Corbin, J. C., H. Czech, D. Massabò, F. B. de Mongeot, G. Jakobi, F. Liu, P. Lobo, C. Mennucci, A. A. Mensah, J. Orasche, et al. 2019. Infrared-absorbing carbonaceous tar can dominate light absorption by marine-engine exhaust. *Npj Clim. Atmos. Sci.* 2 (1):12. doi:10.1038/s41612-019-0069-5.

Cortes, C, and V. Vapnik. 1995. Support-vector networks. *Mach. Learn.* 20 (3):273–97. doi:10.1007/BF00994018.

Cross, E. S., T. B. Onasch, A. Ahern, W. Wrobel, J. G. Slowik, J. Olfert, D. A. Lack, P. Massoli, C. D. Cappa, J. P. Schwarz, et al. 2010. Soot particle studies-instrument inter-comparison-project overview. *Aerosol Sci. Technol.* 44 (8):592–611. doi:10.1080/02786826.2010.482113.

Davies, N. W., C. Fox, K. Szpek, M. I. Cotterell, J. W. Taylor, J. D. Allan, P. I. Williams, J. Trembath, J. M. Haywood, and J. M. Langridge. 2019. Evaluating biases in filter-based aerosol absorption measurements using photoacoustic spectroscopy. *Atmos. Meas. Tech.* 12 (6):3417–34. doi:10.5194/amt-12-3417-2019.

Dobbins, R. A, and C. M. Megaridis. 1991. Absorption and scattering of light by polydisperse aggregates. *Appl. Opt.* 30 (33):4747–54. doi:10.1364/AO.30.004747.

Drucker, H., C. J. C. Burges, L. Kaufman, A. J. Smola, and V. Vapnik. 1997. Support vector regression machines. In *Advances in Neural Information Processing Systems*155–61. Cambridge, MA (United States): MIT Press.

Fierce, L., T. C. Bond, S. E. Bauer, F. Mena, and N. Riemer. 2016. Black carbon absorption at the global scale is affected by particle-scale diversity in composition. *Nat. Commun.* 7:12361. doi:10.1038/ncomms12361.

Fierce, L., T. B. Onasch, C. D. Cappa, C. Mazzoleni, S. China, J. Bhandari, P. Davidovits, D. A. Fischer, T. Helgestad, A. T. Lambe, et al. 2020. Radiative absorption enhancements by black carbon controlled by particle-to-particle heterogeneity in composition. *Proc. Natl. Acad. Sci. USA* 117 (10):5196–203. doi:10.1073/pnas.1919723117.

Forestieri, S. D., T. M. Helgestad, A. T. Lambe, L. Renbaum-Wolff, D. A. Lack, P. Massoli, E. S. Cross, M. K. Dubey, C. Mazzoleni, J. S. Olfert, et al. 2018. Measurement and modeling of the multiwavelength optical properties of uncoated flame-generated soot. *Atmos. Chem. Phys.* 18 (16):12141–59. doi:10.5194/acp-18-12141-2018.

García Fernández, C., S. Picaud, and M. Devel. 2015. Calculations of the mass absorption cross sections for carbonaceous nanoparticles modeling soot. *J. Quant. Spectrosc. Radiat. Transf.* 164:69–81. doi:10.1016/j.jqsrt.2015.05.011.

Gliß, J., A. Mortier, M. Schulz, E. Andrews, Y. Balkanski, S. E. Bauer, A. M. K. Benedictow, H. Bian, R. Checa-Garcia, M. Chin, et al. 2021. AeroCom phase III multi-model evaluation of the aerosol life cycle and optical properties using ground- and space-based remote sensing as well as surface in situ observations. *Atmos. Chem. Phys.* 21 (1):87–128. doi:10.5194/acp-21-87-2021.

Gorham, K. A., S. M. Raffuse, N. P. Hyslop, and W. H. White. 2021. Comparison of recent speciated PM2.5 data from collocated CSN and IMPROVE measurements. *Atmos. Environ.* 244:117977. doi:10.1016/j.atmosenv.2020.117977.

Gyawali, M., W. P. Arnott, R. Zaveri, C. Song, B. Flowers, M. Dubey, A. Setyan, Q. Zhang, S. China, C. Mazzoleni, et al. 2017. Evolution of multispectral aerosol absorption properties in a biogenically-influenced urban environment during the CARES campaign. *Atmosphere (Basel)* 8 (12):217. doi:10.3390/atmos8110217.

He, C., K.-N. Liou, Y. Takano, R. Zhang, M. Levy Zamora, P. Yang, Q. Li, and L. R. Leung. 2015. Variation of the radiative properties during black carbon aging: Theoretical and experimental intercomparison. *Atmos. Chem. Phys.* 15 (20):11967–80. doi:10.5194/acp-15-11967-2015.

Hyslop, N. P, and W. H. White. 2009. Estimating precision using duplicate measurements. *J. Air Waste Manag. Assoc.* 59 (9):1032–9. doi:10.3155/1047-3289.59.9.1032.

Jacobson, M. Z. 2001. Strong radiative heating due to the mixing state of black carbon in atmospheric aerosols. *Nature* 409 (6821):695–7. doi:10.1038/35055518.

Jacobson, M. Z. 2000. A physically-based treatment of elemental carbon optics: Implications for global direct forcing of aerosols. *Geophys. Res. Lett.* 27 (2):217–20. doi:10.1029/1999GL010968.

Knox, A., G. J. Evans, J. R. Brook, X. Yao, C.-H. Jeong, K. J. Godri, K. Sabaliauskas, and J. G. Slowik. 2009. Mass absorption cross-section of ambient black carbon aerosol in relation to chemical age. *Aerosol Sci. Technol.* 43 (6):522–32. doi:10.1080/02786820902777207.

Kondo, Y., H. Matsui, N. Moteki, L. Sahu, N. Takegawa, M. Kajino, Y. Zhao, M. J. Cubison, J. L. Jimenez, S. Vay, et al. 2011. Emissions of black carbon, organic, and inorganic aerosols from biomass burning in North America and Asia in 2008. *J. Geophys. Res.* 116 (D8):D08204. doi:10.1029/2010JD015152.

Lack, D. A, and C. D. Cappa. 2010. Impact of brown and clear carbon on light absorption enhancement, single scatter albedo and absorption wavelength dependence of black carbon. *Atmos. Chem. Phys.* 10 (9):4207–20. doi:10.5194/acp-10-4207-2010.

Lack, D. A, and J. M. Langridge. 2013. On the attribution of black and brown carbon light absorption using the Ångström exponent. *Atmos. Chem. Phys.* 13 (20):10535–43. doi:10.5194/acp-13-10535-2013.

Lack, D. A., H. Moosmüller, G. R. McMeeking, R. K. Chakrabarty, and D. Baumgardner. 2014. Characterizing elemental, equivalent black, and refractory black carbon aerosol particles: A review of techniques, their limitations and uncertainties. *Anal. Bioanal. Chem.* 406 (1):99–122. doi:10.1007/s00216-013-7402-3.

Lesins, G., P. Chylek, and U. Lohmann. 2002. A study of internal and external mixing scenarios and its effect on aerosol optical properties and direct radiative forcing. *J. Geophys. Res.* 107 (D10):AAC5-1–AAC5-12. doi:10.1029/2001JD000973.

Li, H, and A. A. May. 2020a. An exploratory approach using regression and machine learning in the analysis of mass absorption cross section of black carbon aerosols: Model development and evaluation. *Atmosphere (Basel)* 11 (11):1185. doi:10.3390/atmos11111185.

Li, H, and A. A. May. 2020b. Application of regression and machine learning approaches in the analysis of mass absorption cross section of black carbon aerosols. Zenodo. //zenodo.org/record/3967833.

Li, H., G. R. McMeeking, and A. A. May. 2020. Development of a new correction algorithm applicable to any filter-based absorption photometer. *Atmos. Meas. Tech.* 13 (5):2865–86. doi:10.5194/amt-13-2865-2020.

Li, Z., H. Tan, J. Zheng, L. Liu, Y. Qin, N. Wang, F. Li, Y. Li, M. Cai, Y. Ma, et al. 2019. Light absorption properties and potential sources of particulate brown carbon in the Pearl River Delta region of China. *Atmos. Chem. Phys.* 19 (18):11669–85. doi:10.5194/acp-19-11669-2019.

Liu, C., J. Li, Y. Yin, B. Zhu, and Q. Feng. 2017. Optical properties of black carbon aggregates with non-absorptive coating. *J. Quant. Spectrosc. Radiat. Transf.* 187:443–52. doi:10.1016/j.jqsrt.2016.10.023.

Liu, F., J. Yon, A. Fuentes, P. Lobo, G. J. Smallwood, and J. C. Corbin. 2020. Review of recent literature on the light absorption properties of black carbon: Refractive index, mass absorption cross section, and absorption function. *Aerosol Sci. Technol.* 54 (1):33–51. doi:10.1080/02786826.2019.1676878.

Liu, S., A. C. Aiken, K. Gorkowski, M. K. Dubey, C. D. Cappa, L. R. Williams, S. C. Herndon, P. Massoli, E. C. Fortner, P. S. Chhabra, et al. 2015. Enhanced light absorption by mixed source black and brown carbon particles in UK winter. *Nat. Commun.* 6:8435. doi:10.1038/ncomms9435.

May, A. A, and H. Li. 2022. Application of machine learning approaches in the analysis of mass absorption cross-section of black carbon aerosols: Sensitivity analyses and wavelength dependencies. *Aerosol Sci. Technol.* doi:10.1080/02786826.2022.2114312

May, A. A., G. R. McMeeking, T. Lee, J. W. Taylor, J. S. Craven, I. Burling, A. P. Sullivan, S. Akagi, J. L. Collett, M. Flynn, et al. 2014. Aerosol emissions from prescribed fires in the United States: A synthesis of laboratory and aircraft measurements. *J. Geophys. Res. Atmos.* 119 (20):11826–11849. doi:10.1002/2014JD021848.

Mbengue, S., N. Zikova, J. Schwarz, P. Vodička, A. H. Šmejkalová, and I. Holoubek. 2021. Mass absorption cross-section and absorption enhancement from long term black and elemental carbon measurements: A rural background station in Central Europe. *Sci. Total Environ.* 794:148365. doi:10.1016/j.scitotenv.2021.148365.

McDuffie, E. E., S. J. Smith, P. O'Rourke, K. Tibrewal, C. Venkataraman, E. A. Marais, B. Zheng, M. Crippa, M. Brauer, and R. V. Martin. 2020. A global anthropogenic emission inventory of atmospheric pollutants from sector- and fuel-specific sources (1970–2017): An application of the community emissions data system (CEDS). *Earth Syst. Sci. Data.* 12 (4):3413–42. doi:10.5194/essd-12-3413-2020.

Moosmüller, H., W. P. Arnott, C. F. Rogers, J. C. Chow, C. A. Frazier, L. E. Sherman, and D. L. Dietrich. 1998. Photoacoustic and filter measurements related to aerosol light absorption during the northern front range air quality study (Colorado 1996/1997). *J. Geophys. Res.* 103 (D21):28149–57. doi:10.1029/98JD02618.

Moteki, N., Y. Kondo, and K. Adachi. 2014. Identification by single-particle soot photometer of black carbon particles attached to other particles: Laboratory experiments and ground observations in Tokyo. *J. Geophys. Res. Atmos.* 119 (2):1031–43. doi:10.1002/2013JD020655.

Nordmann, S., W. Birmili, K. Weinhold, K. Müller, G. Spindler, and A. Wiedensohler. 2013. Measurements of the mass absorption cross section of atmospheric soot particles using Raman spectroscopy. *J. Geophys. Res. Atmos.* 118 (21):12075–12085. doi:10.1002/2013JD020021.

Ogren, J. A., J. Wendell, E. Andrews, and P. J. Sheridan. 2017. Continuous light absorption photometer for long-term studies. *Atmos. Meas. Tech.* 10 (12):4805–18. doi:10.5194/amt-10-4805-2017.

Ohata, S., T. Mori, Y. Kondo, S. Sharma, A. Hyvärinen, E. Andrews, P. Tunved, E. Asmi, J. Backman, H. Servomaa, et al. 2021. Estimates of mass absorption cross sections of black carbon for filter-based absorption photometers in the Arctic. *Atmos. Meas. Tech.* 14 (10):6723–48. doi:10.5194/amt-14-6723-2021.

Petzold, A., J. A. Ogren, M. Fiebig, P. Laj, S.-M. Li, U. Baltensperger, T. Holzer-Popp, S. Kinne, G. Pappalardo, N. Sugimoto, et al. 2013. Recommendations for reporting "black carbon" measurements. *Atmos. Chem. Phys.* 13 (16):8365–79. doi:10.5194/acp-13-8365-2013.

Ram, K, and M. M. Sarin. 2009. Absorption coefficient and site-specific mass absorption efficiency of elemental carbon in aerosols over urban, rural, and high-altitude sites in India. *Environ. Sci. Technol.* 43 (21):8233–9. doi:10.1021/es9011542.

Saliba, G., R. Subramanian, R. Saleh, A. T. Ahern, E. M. Lipsky, A. Tasoglou, R. C. Sullivan, J. Bhandari, C.

Mazzoleni, and A. L. Robinson. 2016. Optical properties of black carbon in cookstove emissions coated with secondary organic aerosols: Measurements and modeling. *Aerosol Sci. Technol.* 50 (11):1264–76. doi:10.1080/02786826.2016.1225947.

Saturno, J., C. Pöhlker, D. Massabò, J. Brito, S. Carbone, Y. Cheng, X. Chi, F. Ditas, I. Hrab De Angelis, D. Morán-Zuloaga, et al. 2017. Comparison of different aethalometer correction schemes and a reference multi-wavelength absorption technique for ambient aerosol data. *Atmos. Meas. Tech.* 10 (8):2837–50. doi:10.5194/amt-10-2837-2017.

Scarnato, B. V., S. Vahidinia, D. T. Richard, and T. W. Kirchstetter. 2013. Effects of internal mixing and aggregate morphology on optical properties of black carbon using a discrete dipole approximation model. *Atmos. Chem. Phys.* 13 (10):5089–101. doi:10.5194/acp-13-5089-2013.

Schnaiter, M., C. Linke, O. Möhler, K. Naumann, H. Saathoff, R. Wagner, U. Schurath, and B. Wehner. 2005. Absorption amplification of black carbon internally mixed with secondary organic aerosol. *J. Geophys. Res.* 110 (D19):D19204. doi:10.1029/2005JD006046.

Schumacher, R. S., D. A. Hence, S. W. Nesbitt, R. J. Trapp, K. A. Kosiba, J. Wurman, P. Salio, M. Rugna, A. C. Varble, and N. R. Kelly. 2021. Convective-storm environments in subtropical South America from high-frequency soundings during RELAMPAGO-CACTI. *Mon. Weather Rev.* 149 (5):1439–58. doi:10.1175/MWR-D-20-0293.1.

Smola, A. J, and B. Schölkopf. 1998. On a kernel-based method for pattern recognition, regression, approximation, and operator inversion. *Algorithmica* 22 (1–2): 211–31. doi:10.1007/PL00013831.

Sorensen, C. M. 2001. Light scattering by fractal aggregates: A review. *Aerosol Sci. Technol.* 35 (2):648–87. doi:10.1080/02786820117868.

Srivastava, P., M. Naja, T. R. Seshadri, H. Joshi, U. C. Dumka, M. M. Gogoi, and S. S. Babu. 2021. Implications of site-specific mass absorption cross-section (MAC) to black carbon observations at a high-altitude site in the Central Himalaya. *Asia-Pacific J. Atmos. Sci.* 48 (1):83–96. doi:10.1007/s13143-021-00241-6.

Stein, A. F., R. R. Draxler, G. D. Rolph, B. J. B. Stunder, M. D. Cohen, and F. Ngan. 2015. NOAA's HYSPLIT atmospheric transport and dispersion modeling system. *Bull. Am. Meteorol. Soc.* 96 (12):2059–77. doi:10.1175/BAMS-D-14-00110.1.

Subramanian, R., G. L. Kok, D. Baumgardner, A. Clarke, Y. Shinozuka, T. L. Campos, C. G. Heizer, B. B. Stephens, B. de Foy, P. B. Voss, et al. 2010. Black carbon over Mexico: The effect of atmospheric transport on mixing state, mass absorption cross-section, and BC/CO ratios. *Atmos. Chem. Phys.* 10 (1):219–37. doi:10.5194/acp-10-219-2010.

Sumlin, B. J., W. R. Heinson, and R. K. Chakrabarty. 2018. Retrieving the aerosol complex refractive index using PyMieScatt: A Mie computational package with visualization capabilities. *J. Quant. Spectrosc. Radiat. Transf.* 205: 127–34. doi:10.1016/j.jqsrt.2017.10.012.

Varoquaux, G., G. Emmanuelle, O. Vahtras, H. P. R. Valentin, and E. Al. 2015. Scipy lecture notes: One document to learn numerics, science, and data with Python.

Wang, Y., Y. Pang, J. Huang, L. Bi, H. Che, X. Zhang, and W. Li. 2021. Constructing shapes and mixing structures of black carbon particles with applications to optical calculations. *J. Geophys. Res. Atmos.* 126 (10). doi:10.1029/2021JD034620.

Wei, X., Y. Zhu, J. Hu, C. Liu, X. Ge, S. Guo, D. Liu, H. Liao, and H. Wang. 2020. Recent progress in impacts of mixing state on optical properties of black carbon aerosol. *Curr. Pollution Rep.* 6 (4):380–98. doi:10.1007/s40726-020-00158-0.

Wu, Y., T. Cheng, D. Liu, J. D. Allan, L. Zheng, and H. Chen. 2018. Light absorption enhancement of black carbon aerosol constrained by particle morphology. *Environ. Sci. Technol.* 52 (12):6912–9. doi:10.1021/acs.est.8b00636.

Xu, X., W. Zhao, X. Qian, S. Wang, B. Fang, Q. Zhang, W. Zhang, D. S. Venables, W. Chen, Y. Huang, et al. 2018. The influence of photochemical aging on light absorption of atmospheric black carbon and aerosol single-scattering albedo. *Atmos. Chem. Phys.* 18 (23):16829–44. doi:10.5194/acp-18-16829-2018.

Yuan, J., R. L. Modini, M. Zanatta, A. B. Herber, T. Müller, B. Wehner, L. Poulain, T. Tuch, U. Baltensperger, and M. Gysel-Beer. 2021. Variability in the mass absorption cross section of black carbon (BC) aerosols is driven by BC internal mixing state at a central European background site (Melpitz, Germany) in winter. *Atmos. Chem. Phys.* 21 (2):635–55. doi:10.5194/acp-21-635-2021.

Zanatta, M., M. Gysel, N. Bukowiecki, T. Müller, E. Weingartner, H. Areskoug, M. Fiebig, K. E. Yttri, N. Mihalopoulos, G. Kouvarakis, et al. 2016. A European aerosol phenomenology-5: Climatology of black carbon optical properties at 9 regional background sites across Europe. *Atmos. Environ* 145:346–64. doi:10.1016/j.atmosenv.2016.09.035.

Zanatta, M., P. Laj, M. Gysel, U. Baltensperger, S. Vratolis, K. Eleftheriadis, Y. Kondo, P. Dubuisson, V. Winiarek, S. Kazadzis, et al. 2018. Effects of mixing state on optical and radiative properties of black carbon in the European Arctic. *Atmos. Chem. Phys.* 18 (19):14037–57. doi:10.5194/acp-18-14037-2018.

Zaveri, R. A., J. C. Barnard, R. C. Easter, N. Riemer, and M. West. 2010. Particle-resolved simulation of aerosol size, composition, mixing state, and the associated optical and cloud condensation nuclei activation properties in an evolving urban plume. *J. Geophys. Res.* 115 (D17): D17210. doi:10.1029/2009JD013616.

Zhang, R., A. F. Khalizov, J. Pagels, D. Zhang, H. Xue, and P. H. McMurry. 2008. Variability in morphology, hygroscopicity, and optical properties of soot aerosols during atmospheric processing. *Proc. Natl. Acad. Sci. USA.* 105 (30):10291–6. doi:10.1073/pnas.0804860105.

Zhang, X., M. Mao, Y. Yin, and B. Wang. 2018. Numerical investigation on absorption enhancement of black carbon aerosols partially coated with nonabsorbing organics. *J. Geophys. Res. Atmos.* 123 (2):1297–308. doi:10.1002/2017JD027833.

Zhang, X., M. Mao, Y. Yin, and B. Wang. 2017. Absorption enhancement of aged black carbon aerosols affected by their microphysics: A numerical investigation. *J. Quant. Spectrosc. Radiat. Transf.* 202:90–7. doi:10.1016/j.jqsrt.2017.07.025.